Nondipole asymmetries of Kr 1s photoelectrons

B. Krässig, J.-C. Bilheux,* R. W. Dunford, D. S. Gemmell,
S. Hasegawa,† E. P. Kanter, S. H. Southworth, and L. Young
Argonne National Laboratory, Argonne, Illinois 60439

L. A. LaJohn and R. H. Pratt
Department of Physics and Astronomy,
University of Pittsburgh, Pittsburgh, Pennsylvania 15260

(Dated: September 26, 2002)

Abstract

Nondipole asymmetries of Kr 1s photoelectrons were measured over the 11–8000 eV kinetic energy range. Symmetry properties of angular distributions were exploited to eliminate the dependence of the measurements on the dipole anisotropy and the polarization properties of the photon beam. The measured asymmetries agree well with both full multipole relativistic and nonrelativistic first-order retardation calculations within the independent-particle approximation. Deviations of the measured asymmetries from predictions of the point-Coulomb retardation correction confirm the importance of screening on the continuum-wave normalizations and phase shifts.

PACS numbers: 32.80.Fb, 33.60.Fy

*Present address: Oak Ridge National Laboratory, Oak Ridge, Tennessee 37831
†Present address: Department of Quantum Engineering and Systems Science, University of Tokyo, Tokyo 113-8656, Japan

I. INTRODUCTION

The dipole approximation to the photon-electron interaction is often adopted in atomic photoionization studies to describe angle-integrated cross sections and the dipole anisotropy parameter [1, 2]. Nondipole interactions produce additional asymmetries in photoelectron angular distributions that have long been studied experimentally and theoretically [3]. The early theories, for example the retardation correction to the angular distribution of 1s photoelectrons in the point Coulomb potential [4], predict nondipole asymmetries to vary as v/c, i.e., for angular distributions to be skewed increasingly "forward" with respect to the photon propagation vector as the photoelectron velocity v increases. In modern theories, photoionization amplitudes are calculated in screened potentials, and richer Z-dependent and subshell-dependent energy variations of nondipole asymmetries are obtained [5–11].

The nonrelativistic expression for the photoionization matrix element between the bound state $|i\rangle$ and continuum state $|f\rangle$ is

$$M_{if} = \langle f| \exp(i\mathbf{k}\cdot\mathbf{r})\boldsymbol{\epsilon}\cdot\mathbf{p}|i\rangle, \tag{1}$$

where $\mathbf{k}$ is the photon propagation vector, $\mathbf{r}$ is the electron position vector, $\boldsymbol{\epsilon}$ is the linear-polarization vector of the photon, and $\mathbf{p}$ is the electron momentum operator. The differential cross section is proportional to $|M_{if}|^2$ and, in general, depends on the angles between the photoelectron momentum vector and both $\boldsymbol{\epsilon}$ and $\mathbf{k}$. Atomic photoionization can be treated in a full relativistic multipole expansion within the independent-particle approximation (IPA). For example, Tseng *et al.* [5] discussed relativistic, multipole, and screening effects, and compared their calculations with existing experiments. While that theory is complete within the IPA, leading correction terms to the dipole approximation can be included by adopting the "retardation expansion" of the exponential factor in Eq. (1):

$$\exp(i\mathbf{k}\cdot\mathbf{r}) \approx 1 + i\mathbf{k}\cdot\mathbf{r} - \frac{1}{2}(\mathbf{k}\cdot\mathbf{r})^2 + ... \tag{2}$$

The retardation expansion [6, 7] is not the same as the multipole expansion [12]. Treating a finite number of terms in Eq. (2) includes a finite number of multipoles within the long-wavelength limit ($\mathrm{k} \to 0$). Keeping only the leading term, $\exp(i\mathbf{k}\cdot\mathbf{r}) \approx 1$, is the "non-retarded dipole approximation" and treats the photon-electron interaction as an electric-dipole (E1) process in the long-wavelength limit. Since there is no dependence on the direction of $\mathbf{k}$

in the dipole approximation, calculated angular distributions are symmetric with respect to reversal of $\mathbf{k}$.

The "first retardation correction" consists in keeping the second term in the expansion, $\exp(i\mathbf{k}\cdot\mathbf{r}) \approx 1 + i\mathbf{k}\cdot\mathbf{r}$, which introduces long-wavelength limits of electric-quadrupole (E2) and magnetic-dipole (M1) interactions. Retaining terms to order kr in calculations of $|M_{if}|^2$ then includes E1-E2 and E1-M1 cross terms, i.e., interference between E1 photoionization amplitudes and those for E2 and M1 interactions, but excludes E2-E2, M1-M1, and E2-M1 terms that are of order $(\mathrm{kr})^2$. The E1-E2 and E1-M1 cross terms have odd parity and produce asymmetries in angular distributions with respect to reversal of the direction of $\mathbf{k}$. For photoionization of randomly-oriented atoms by a linearly-polarized photon beam and including terms up to first order in kr, the differential cross section can be expressed as [9]

$$\frac{d\sigma}{d\Omega}(\theta,\phi) = \frac{\sigma}{4\pi}\left\{1 + \beta P_2(\cos\theta) + (\delta + \gamma\cos^2\theta)\sin\theta\cos\phi\right\}, \tag{3}$$

where σ is the angle-integrated cross section, β is the dipole anisotropy parameter, $P_2(\cos\theta) = (3\cos^2\theta - 1)/2$ is the second Legendre polynomial, and δ and γ parameterize the nondipole asymmetries resulting from E1-E2 and E1-M1 cross terms. The coordinate axes for Eq. (3) are shown in Fig. 1, with the positive x axis along the direction of $\mathbf{k}$, the z axis along the linear polarization vector $\boldsymbol{\epsilon}$, and θ and ϕ are the polar and azimuthal angles of the photoelectron momentum vector. Retaining the third term in Eq. (2) includes long-wavelength limits of electric-octupole (E3) and magnetic-quadrupole (M2) interactions and retardation corrections to electric-dipole amplitudes [10].

Tunable synchrotron radiation has been used in recent years to measure the variations of nondipole asymmetries with energy and atomic subshell. The measurements for Ne 2s [13], Ar 1s [14], and Kr 2s and 2p [15] are in generally good agreement with first-order retardation calculations. However, the second-order terms E1-E3 and E2-E2 were included to explain the Ne 2p asymmetries measured at kinetic energies higher than 800 eV [13].

Here we report on an experimental and theoretical study of nondipole asymmetries of Kr 1s photoelectrons over the 11–8000 eV kinetic energy range ($\hbar\omega \approx 14.3 - 22.3$ keV). The measurements were made with an electron spectrometer utilizing four analyzers positioned at angles that allow determination of nondipole asymmetries independent of the dipole anisotropy and the polarization properties of the photon beam. The dipole anisotropy was also mapped out at 996 eV kinetic energy by rotating the analyzers through their full angular

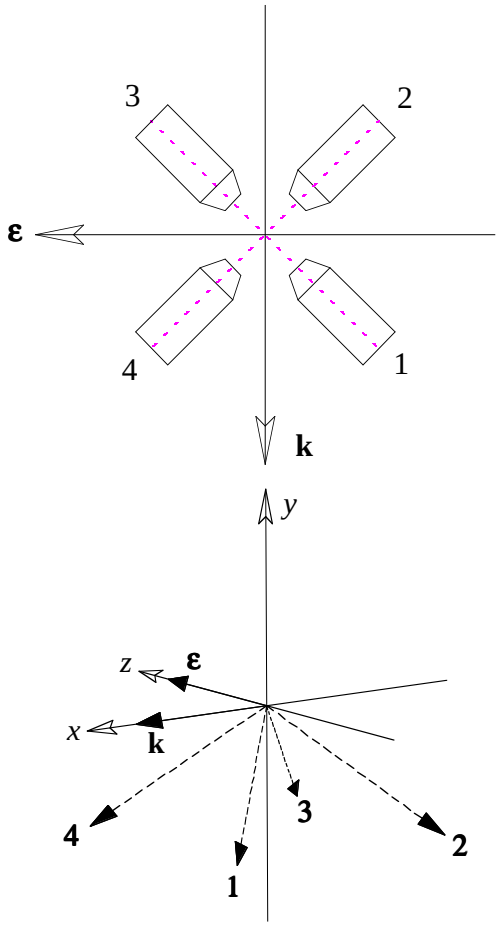

FIG. 1: Angular positions of the four electron analyzers, labeled 1-4, with respect to the propagation vector $\mathbf{k}$ and polarization vector $\boldsymbol{\epsilon}$ of the photon beam. The bottom figure shows a trimetric view and the top figure shows a projection in the $\boldsymbol{\epsilon} - \mathbf{k}$ plane.

range. The measured nondipole asymmetries are compared with full multipole relativistic IPA calculations and with first-order retardation nonrelativistic IPA calculations [6]. Comparison with the point-Coulomb retardation correction confirms the importance of screening on the continuum-wave normalizations and phase shifts.

II. EXPERIMENTAL METHODS

A. Symmetry properties of angular distributions

Measurements of photoelectron angular distributions can be complicated by incomplete polarization of the photon beam and misalignment of the experimental geometry with the polarization direction [15]. For example, bending-magnet sources of synchrotron radiation are elliptically polarized, and reflections from beamline optics can affect the degree of polarization and introduce a tilt of the polarization ellipse with respect to the storage-ring orbital plane [16]. Peshkin [17] has shown that these difficulties can be eliminated by exploiting symmetry properties of angular distributions imposed by the intrinsic symmetry properties of photons. The general form of the differential cross section, with angles (θ', ϕ') referenced to $\mathbf{k}$, can be expressed as an expansion in spherical harmonics $Y_{LM}(\theta', \phi')$:

$$\frac{d\sigma}{d\Omega}(\theta', \phi') = \frac{\sigma}{4\pi} \sum_{L,M} b_{LM} Y_{LM}(\theta', \phi'), \tag{4}$$

where σ is the angle-integrated cross section and the coefficients b_{LM} contain dynamical information (photoionization amplitudes) and depend on the polarization state of the photon beam [12]. The range of L values in Eq. (4) is determined by the number and type of multipoles included in specific calculations, but the M values are restricted to $0, \pm 2$ by the unit spin, odd intrinsic parity, and transversality properties of photons. Using a density matrix description of the photon polarization state, Peshkin has shown that the average of $\frac{d\sigma}{d\Omega}(\theta', \phi')$ with $\frac{d\sigma}{d\Omega}(\theta', \phi' + 90°)$ is independent of the polarization state of the photon beam and equal to that for an unpolarized beam at polar angle θ'. We use this symmetry property in the measurement method described in the next section.

Our data analysis yields photoelectron intensities corresponding to an unpolarized photon beam. For an unpolarized beam, angular distributions are rotationally symmetric about $\mathbf{k}$ and depend only on the angle θ' between $\mathbf{k}$ and the photoelectron momentum vector. The general form of the differential cross section for an unpolarized photon beam can be expressed as [5]

$$\frac{d\sigma}{d\Omega}(\theta') = \frac{\sigma}{4\pi} \sum_{n=0}^{\infty} B_n P_n(\cos\theta'), \tag{5}$$

where the $P_n(\cos\theta')$ are Legendre polynomials and $B_0 = 1$. The orders n of the Legendre polynomials are the same as the L values in Eq. (4) and are determined by the number and

type of multipoles included in the theory. The asymmetry parameters B_n are determined by the photoionization dynamics. The $n = 0-3$ terms give an expression for the differential cross section equivalent to the first-order retardation expression of Eq. (3):

$$\frac{d\sigma}{d\Omega}(\theta') = \frac{\sigma}{4\pi}\left\{1 + B_1 \cos\theta' + B_2 P_2(\cos\theta') + B_3 P_3(\cos\theta')\right\}, \tag{6}$$

where $B_1 = \delta + \gamma/5$, $B_2 = -\beta/2$, and $B_3 = -\gamma/5$. The $n = 2$ term is an even function of $\cos\theta'$ and describes the dipole anisotropy, while the $n = 1$ and 3 terms are odd functions of $\cos\theta'$ and describe asymmetries with respect to reversal of $\mathbf{k}$. Second-order retardation calculations [10] include the $n = 0 - 4$ terms:

$$\frac{d\sigma}{d\Omega}(\theta') = \frac{\sigma}{4\pi}\left\{1 + B_1 \cos\theta' + B_2 P_2(\cos\theta') + B_3 P_3(\cos\theta') + B_4 P_4(\cos\theta')\right\}. \tag{7}$$

B. Electron spectrometer and beamline

The measurements were made using $\hbar\omega \approx 14.3 - 22.3$ keV x rays on beamline 12-ID at Argonne's Advanced Photon Source [18]. The x-ray beam is highly plane polarized and, in this energy range, the Si(111) double-crystal monochromator and focusing mirror provide a flux $\approx 5\times10^{12}$ s^{-1} in a bandwidth ΔE/E $\approx 4\times10^{-4}$ with a beam cross section ≈ 2 mm^2. The electron spectrometer chamber is double mu-metal shielded to reduce the earth's magnetic field in the interaction region. The spectrometer contains four 45° parallel-plate electron analyzers (PPAs) mounted on a rotation stage with its rotation axis perpendicular to both $\mathbf{k}$ and $\boldsymbol{\epsilon}$ of the x-ray beam. The angular positions of the PPAs are indicated in Fig. 1 and are along the diagonals of a cube whose faces are normal to the coordinate axes. Those angles are "magic" with respect to all three axes, i.e., the direction cosines are all $\pm\frac{1}{\sqrt{3}}$. The angular acceptances of the PPAs are $\Delta\theta' \approx \pm1°$. The PPAs numbered 1 and 4 in Fig. 1 are positioned at the same polar angle, $\theta' = 54.7°$, with respect to $\mathbf{k}$, but their azimuthal angles differ by 90°. The average of the photoelectron intensities at positions 1 and 4, $F \equiv (I_1 + I_4)/2$, is equal to that for an unpolarized photon beam at the "forward" angle $\theta' = 54.7°$. Similarly, the PPAs numbered 2 and 3 are at the same polar angle, $\theta' = 125.3°$, but their azimuthal angles differ by 90°. The average of the photoelectron intensities at positions 2 and 3, $B \equiv (I_2 + I_3)/2$, is equal to that for an unpolarized photon beam at the "backward" angle $\theta' = 125.3°$. We define the difference between the photoelectron intensities measured at $\theta' = 54.7°$ and 125.3° divided by their sum to be the experimental nondipole

asymmetry $A \equiv (F - B)/(F + B)$. Since $B_2 P_2(\cos\theta') = 0$ at magic angles, A is insensitive to the dipole anisotropy. Comparison with a first-order nondipole calculation expressed by Eq. (6) gives

$$A = \frac{1}{\sqrt{3}}(B_1 - \frac{2}{3}B_3), \tag{8}$$

and comparison with a second-order calculation expressed by Eq. (7) gives

$$A = \frac{1}{\sqrt{3}} \left\{ \frac{B_1 - \frac{2}{3}B_3}{1 - \frac{7}{18}B_4} \right\}. \tag{9}$$

Variations of collection efficiencies among the four PPAs are accounted for by rotating the mounting stage to measure photoelectron intensities with each PPA at each of the four angular positions, and the results are averaged. Averaging also reduces systematic errors due to residual fields and small angular misalignments. Using the symmetry property described in the previous subsection eliminates the need to accurately determine the degree of linear polarization of the photon beam and the tilt of the polarization ellipse [15]. However, the PPA rotation axis must be perpendicular to $\mathbf{k}$ to avoid introducing a systematic forward-backward asymmetry [19]. Accurate alignment with respect to $\mathbf{k}$ is established by apertures for the photon beam that are optically aligned with machined reference apertures mounted on the PPA rotation stage. The PPAs accept electrons emitted from a common source volume produced by the intersection of the photon beam with an effusive gas jet, and the four PPA positions view equivalent solid angles. A flow control valve maintains constant gas density. The photoelectron signals were normalized to the intensity of Kr K x-ray fluorescence measured by a NaI scintillation detector to account for variations in x-ray beam flux and overlap between the x rays and gas jet. The Kr 1s photoabsorption edge was located by recording the x-ray fluorescence yield while scanning the beamline monochromator. Energies were referenced to the ionization threshold at 14327.2(8) eV [20].

III. RESULTS AND DISCUSSION

A. Dipole anisotropy

While the focus of our study is measurement of the Kr 1s nondipole asymmetry, we also measured the dipole anisotropy at one energy by rotating the PPAs through their full angular range and recording photoelectron intensities as a function of the angles between

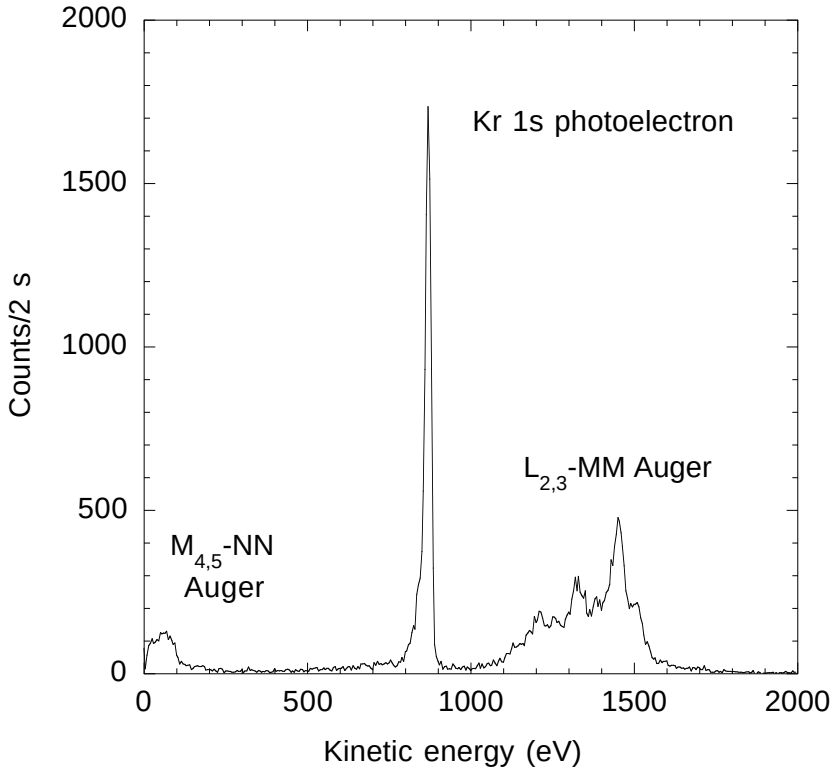

FIG. 2: Kr 1s photoelectron and Auger electron spectrum recorded using 15181 eV x rays. The spectrum is uncorrected for the collection efficiencies of the electron analyzers, which are proportional to kinetic energy.

the photoelectron momentum vector and both $\boldsymbol{\epsilon}$ and $\mathbf{k}$. In that case, it is useful to define our coordinate axes with x along $\mathbf{k}$, y along $\boldsymbol{\epsilon}$, and z along the vertical PPA rotation axis, because the PPAs are then positioned at fixed polar angle $\theta'' = 125.3°$ and variable azimuthal angle ϕ'' (the angular positions 1, 2, 3, 4 indicated in Fig. 1 are $\phi'' = 45°, 135°, 225°, 315°$, respectively). Shaw *et al.* [19] discussed the advantages of this measurement geometry and gave the form of the angular distribution with first-order retardation parameters. In the present case of Kr 1s, the nondipole asymmetry parameter $\delta = 0$ in a nonrelativistic model and is very small in relativistic calculations at kinetic energies up to several keV (see [10] and subsection C below). In this case, the angular distribution with first-order retardation included can be expressed as

$$\frac{d\sigma}{d\Omega}(\phi'') = \frac{\sigma}{4\pi}\left\{1 + \beta(\sin^2\phi'' - 1/2) + \gamma(\sqrt{\frac{8}{27}}\sin^2\phi''\cos\phi'')\right\}. \qquad (10)$$

Figure 2 shows a Kr 1s photoelectron spectrum and the $L_{2,3}$-MM and $M_{4,5}$-NN Auger-

electron spectra recorded using 15181 eV x rays. The spectrum is summed over the four PPAs and is uncorrected for their collection efficiencies, which are proportional to kinetic energy. We measured the Kr 1s photoelectron count rate vs. rotation angle ϕ'' at 996 eV kinetic energy. The potentials on the PPAs were set to accept electron energies at the maximum of the photoelectron peak with 25 eV resolution, and electrons were counted over $\phi'' = 0 - 360°$ in 10° steps. A similar data set was recorded for $L_{2,3}$-MM Auger electrons at 1460 eV with 36 eV resolution. All measurements were normalized to the intensity of x-ray fluorescence recorded by the NaI detector. The intensities from the four PPAs were summed at corresponding angles ϕ''. At photon energies far above threshold, it is a good approximation to assume that Auger-electron emission proceeds as a second-step process independent of the photoionization step. Auger electrons then have zero first-order nondipole asymmetries [21], but they could have dipole anisotropies due to alignment of vacancy states [16]. However, we assume here that the $L_{2,3}$ vacancies are produced primarily by $K \rightarrow L_{2,3}$ vacancy transfers. Since the initially formed K vacancies cannot be aligned, all fluorescent photons and Auger electrons are emitted isotropically in the limit of a multi-step photoabsorption and decay process. We therefore interpret our measurement of a $\pm 5\%$ variation of the Auger electron count rate with angle to be due to small variations of the observed source volume or other instrumental effects.

The Kr 1s photoelectron count rate vs. ϕ'' was corrected for the $\pm 5\%$ instrumental variation, and the results are plotted in Fig. 3 along with a fitted curve based on Eq. 10. The measurements are sensitive to the degree of linear polarization of the x-ray beam and the tilt of the polarization axis with respect to the PPA rotation stage. Eq. (10) can be modified to include those instrumental parameters [15, 19], but a good fit to the data was obtained under the assumptions of 100% polarization and zero tilt. At 996 eV, the nondipole asymmetry parameter $\gamma \approx 0$ (see following subsection), and it can be seen that the data are approximately symmetric between the "forward" angles ($\phi'' = 0 - 180°$) and the "backward" angles ($\phi'' = 180 - 360°$). The fitted curve assumes $\gamma = 0$ and gives $\beta = 1.95(2)$, in fair agreement with the nonrelativistic value $\beta = 2$. Our relativistic IPA calculation predicts $\beta = 1.99$ at this energy. This measurement demonstrates the dominant dipole character of the Kr 1s angular distribution at this energy. In principle, this multi-angle measurement method allows simultaneous determination of dipole anisotropies and nondipole asymmetries if the polarization properties of the photon beam are known.

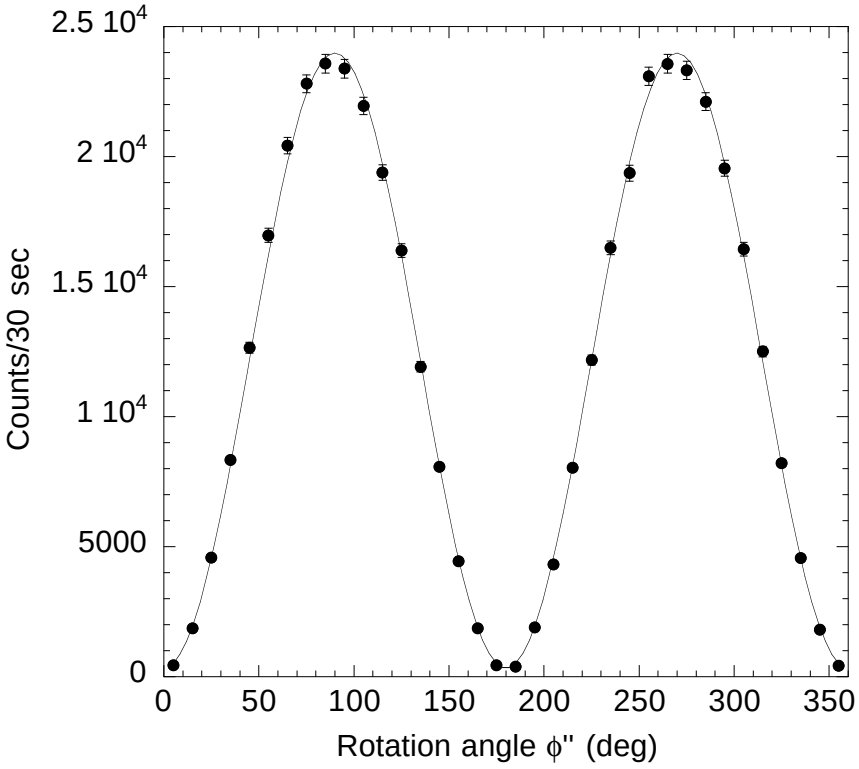

FIG. 3: Angular distribution of Kr 1s photoelectrons at 996 eV kinetic energy. The measurements are plotted as solid circles, and the fitted curve yields a dipole anisotropy parameter $\beta = 1.95(2)$.

B. Nondipole asymmetries

Nondipole asymmetries A were measured for Kr 1s photoelectrons over the 11–8000 eV kinetic energy range and for Auger electrons by the four-angle method described in Section II. In the multi-step model, the first-order nondipole asymmetries of Auger electrons vanish [21]. The Auger electron intensities measured at the four PPA positions varied by $\pm 3\%$ and resulted in very small asymmetries $A = -0.007(4)$ for $M_{4,5}$-NN and $-0.001(4)$ for $L_{2,3}$-MM. The Auger asymmetries were assumed to result from variations in acceptance solid angles or residual fields, and the Kr 1s photoelectron intensities were corrected for these $\pm 3\%$ instrumental effects. To reduce variations of the PPA collection efficiencies at low kinetic energies, data below 40 eV were recorded at a constant pass energy of 30 eV. The data above 40 eV were recorded in nonretarding mode for which the pass energy equals the kinetic energy. The PPA energy resolution was 2.5% of the pass energy.

The measured asymmetries A, with error bars determined by counting statistics, are compared with theory in Fig. 4. At our largest measured $A \approx 0.3$ at 8000 eV, the photoelectron

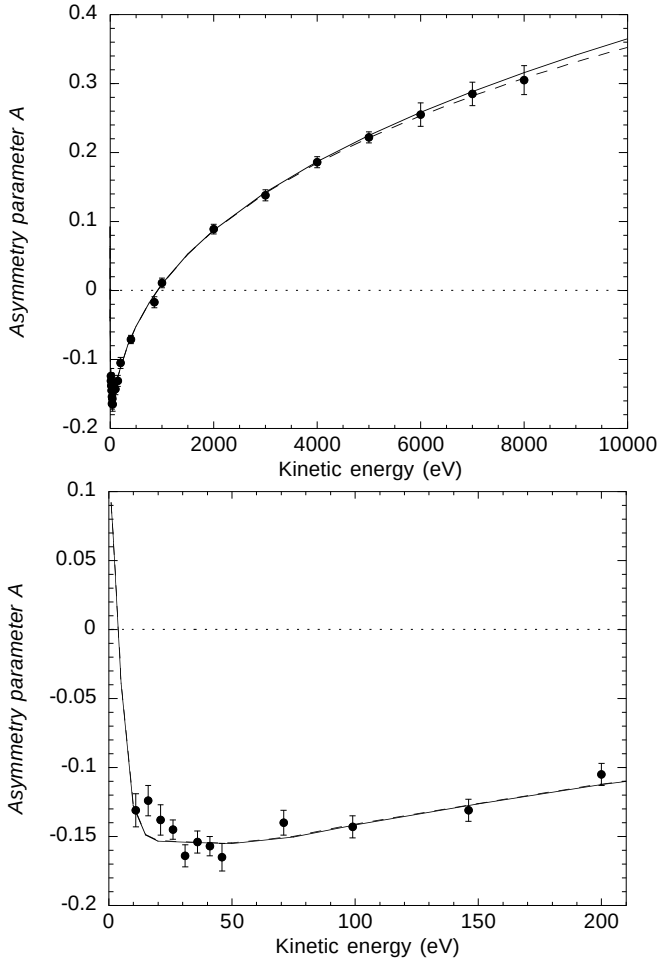

FIG. 4: Measured nondipole asymmetries of Kr 1s photoelectrons (solid circles) compared with relativistic independent-particle calculations of the B_1 and B_3 asymmetry parameters (solid curve). The dashed curve shows the effect of including the B_4 asymmetry parameter. The top figure shows the full set of results while the bottom figure shows the results below 210 eV on an expanded scale.

intensity at $\theta' = 54.7°$ is 85% larger than at 125.3°. Polar plots of calculated differential cross sections at 50, 1000, and 5000 eV are shown in Fig. 5 to illustrate that the angular distribution is tilted backward ($A < 0$) at lower kinetic energies, becomes roughly forward-backward symmetric ($A \approx 0$) near 1000 eV, and is skewed forward ($A > 0$) at high energy. The measured asymmetries are in excellent agreement with relativistic IPA calculations of the B_1 and B_3 parameters of Eq. (8). The B_n parameters were obtained from full relativistic multipole calculations, not the retardation expansion. Including the B_4 parameter in Eq. (9) produces a calculated curve that is distinguishable from Eq. (8) only at very high energies. Since the $B_4 P_4(\cos\theta')$ term in Eq. (7) is an even function of $\cos\theta'$, it affects the

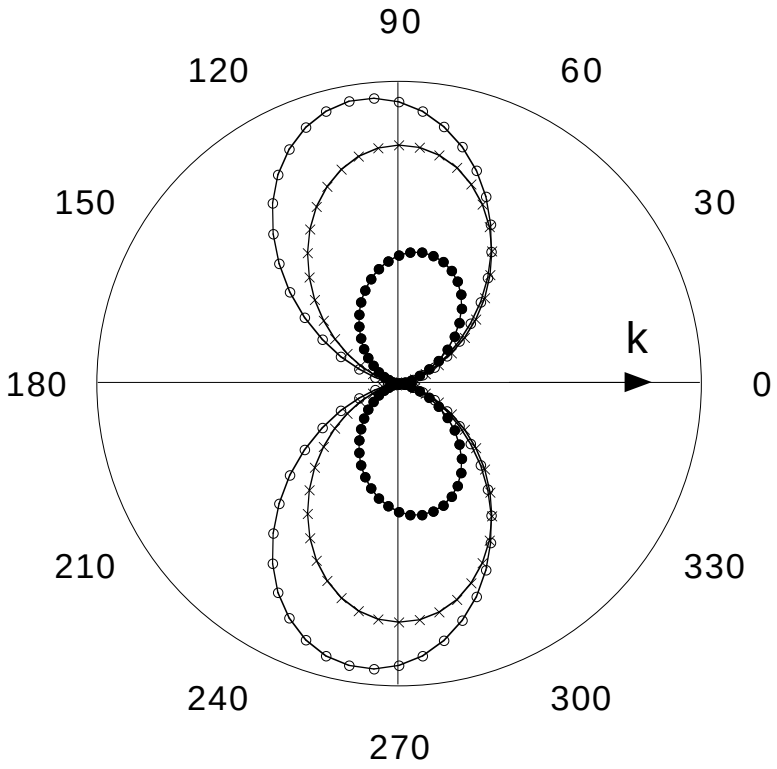

FIG. 5: Polar plot of calculated Kr 1s photoelectron angular distributions showing tilting with respect to the photon propagation vector **k**. The angular distribution is tilted backward at 50 eV (open circles), is approximately forward-backward symmetric at 1000 eV (x's), and is tilted forward at 5000 eV (solid circles). The areas enclosed by the curves are proportional to the angle-integrated cross sections at each energy.

asymmetry A only through the normalization factor of Eq. (9). Although the error bars on the measurements overlap both curves, a χ^2 statistical analysis of the 5–8 keV data favors the second-order calculations of Eq. (9). Our measured and calculated asymmetries are in excellent agreement with the first- and second-order relativistic IPA calculations tabulated in [10].

C. Nonrelativistic first-order retardation model

Key factors that determine the Kr 1s nondipole asymmetry can be explained using the first-order retardation nonrelativistic IPA model discussed in [6]. Two continuum waves are considered, $1s \rightarrow \epsilon p$ and $1s \rightarrow \epsilon d$, produced by E1 and E2 interactions, respectively.

Referring to Eq. (3), this model predicts $\beta = 2$, $\delta = 0$, and γ is determined by interference between the p-wave and d-wave amplitudes. The relativistic IPA B_n parameters used to produce the theoretical curves in Fig. 4 are consistent with this model, giving $\beta > 1.98$ and $|\delta| < 0.0004$ for kinetic energies up to 2000 eV. Using Eq. (6) for the case of unpolarized photons with $B_2 = -1$ and $B_3 = -B_1$ for an s-subshell in a nonrelativistic IPA model, the differential cross section can be expressed in the form used in [6] as

$$\frac{d\sigma}{d\Omega}(\theta') = \frac{3\sigma}{8\pi}\sin^2\theta'(1 + \kappa\cos\theta'), \tag{11}$$

where the parameter $\kappa = \frac{5}{3}B_1 = \gamma/3$ parameterizes the retardation correction, and our measured asymmetry $A = \kappa/\sqrt{3}$. The retardation correction in the point Coulomb model [4] leads to $\kappa \approx 4(v/c)$, where v is the photoelectron velocity [in natural units ($m_e = \hbar = c = 1$)]. The $4(v/c)$ correction is always positive and decreases to zero at threshold, which is inconsistent with the results below 1000 eV in Fig. 4.

Bechler and Pratt [6] explained how use of a screened potential affects calculations of κ between threshold and 2000 eV. In a screened potential, κ varies as $Z\alpha$ at low energies rather than v/c. They define the ratios $n_l \equiv N_l/N_l^c$ of screened to point-Coulomb normalizations of the $l = 1$ and 2 radial continuum functions. Screening also affects the asymptotic phase-shift difference $\delta_2 - \delta_1$ of the continuum functions. Defining $\nu = Z\alpha/p$, where p is the photoelectron momentum, the retardation parameter can be expressed as

$$\kappa = 2\frac{n_2}{n_1}(\nu^2 + 4)^{1/2}\frac{v}{c}\cos(\delta_2 - \delta_1). \tag{12}$$

In the point Coulomb case, $n_2^c/n_1^c = 1$, $\delta_2^c - \delta_1^c = -\arctan(\nu/2)$ [22], and at low energies, $\nu \gg 1$, $\delta_2^c - \delta_1^c \approx -\pi/2 + 2/\nu$ [22], $\cos(\delta_2^c - \delta_1^c) \approx 2/\nu$, and $\kappa \approx 4(v/c)$. Screening modifies the continuum normalizations and phase shifts, shown in Fig. 6, and produces good agreement with measured values of κ, shown in Fig. 7.

In Fig. 6, the calculated maximum in n_2/n_1 near 7 eV and corresponding rapid variation of $\cos(\delta_2 - \delta_1)$ are suggestive of a shape resonance. Additional calculations confirmed the presence of an IPA shape resonance in the d-wave channel. While the phase of the p wave changes slowly, the phase of the d wave varies rapidly and produces strong variation of $\cos(\delta_2 - \delta_1)$ in the $\approx 1 - 10$ eV region. Since the sign of κ is determined by $\cos(\delta_2 - \delta_1)$, this phase-shift change drives κ from positive to negative over that energy range. Above the resonance region, $\cos(\delta_2 - \delta_1)$ and κ slowly vary from negative to positive, passing through

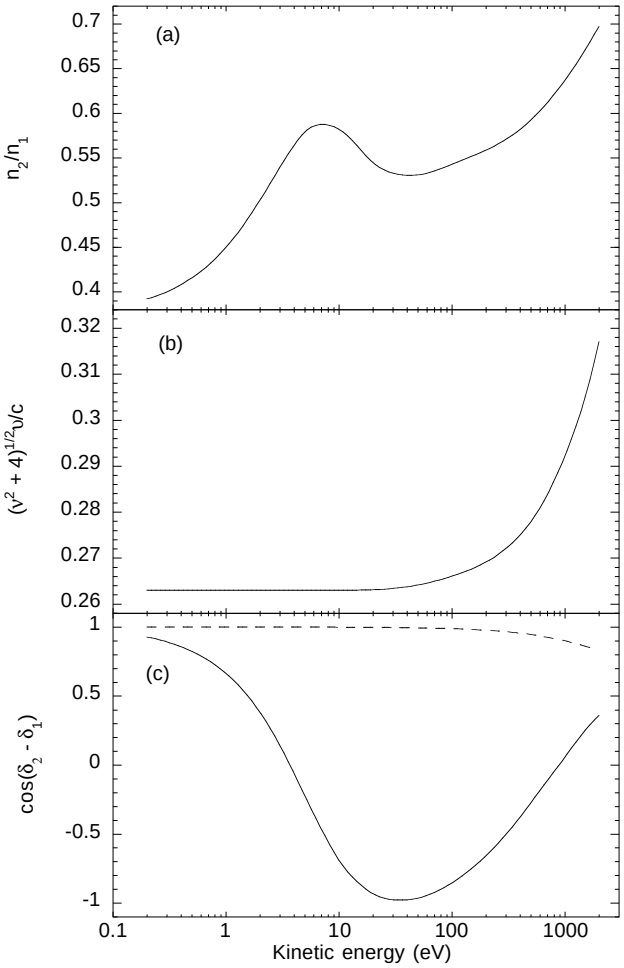

FIG. 6: Calculated factors that determine the retardation correction parameter κ for Kr 1s photoelectrons. (a) The effect of screening on normalizations of continuum functions. (b) Photoelectron velocity factor. (c) Phase-shift factor for point Coulomb (dashed curve) and screened potentials (solid curve). See text for explanations.

zero near 1000 eV. Unfortunately, attempts to measure the nondipole asymmetry in the 1–10 eV resonance region were unsuccessful due to the Auger background and, perhaps, distortions of the electron spectra caused by post-collision interaction.

Good agreement of the nonrelativistic IPA first-order retardation calculation with measurements (Fig. 7) indicates that while screening is an important factor at these energies, electron correlation and relativity apparently are not. The nondipole asymmetries of outer subshells can be strongly affected by electron correlation with inner subshells, both at low kinetic energies [11] and at energies far above threshold [23]. In the Kr 1s case, there are no deeper subshells and the 1s IPA cross section is large compared with those of the outer sub-

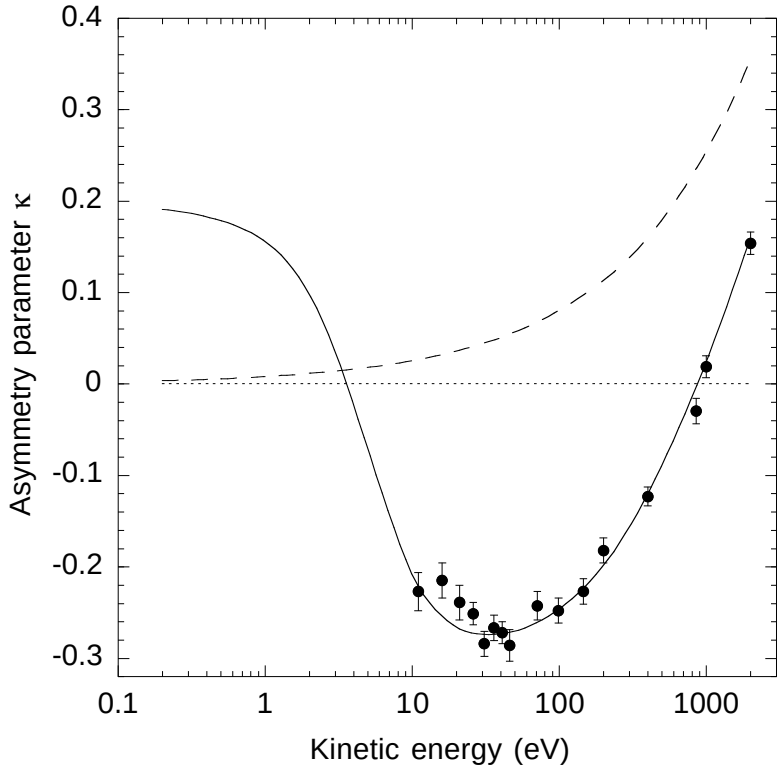

FIG. 7: Retardation correction parameter κ for Kr 1s photoelectrons. The measurements (solid circles) are compared with first-order retardation nonrelativistic independent-particle calculations with screening (solid curve) and the $4(v/c)$ prediction of the point Coulomb model (dashed curve).

shells, so significant electron correlation is less likely. However, we were unable to measure below 11 eV, and electron correlation is generally expected to be significant within a few eV of threshold. Relativity is also apparently not important for Kr 1s in the energy region measured here. The dipole character of the angular distribution is largely retained, with the dipole lobes skewed backward or forward as shown in Fig. 5, and the angular distribution can be parameterized with the first few B_n parameters. In the relativistic regime, the angular distributions of high-Z atoms at energies of hundreds of keV are pushed far forward, filling in the minimum at 0°, and the expansion of Eq. 5 converges slowly [5].

IV. CONCLUSION

Nondipole asymmetries of Kr 1s photoelectrons were measured over the 11–8000 eV kinetic energy range using an experimental method that is insensitive to the dipole anisotropy

and the polarization state of the photon beam. The dipole anisotropy was also mapped out at 996 eV. The measured nondipole asymmetries agree well with full relativistic multipole calculations in the independent-particle approximation. The measurements also agree well with nonrelativistic first-order retardation calculations between threshold and 2000 eV, where strong deviations from the point Coulomb model are attributed to screening effects on the normalizations and asymptotic phase shifts of the continuum functions.

V. ACKNOWLEDGEMENTS

We are grateful to the staff of the Basic Energy Sciences Synchrotron Radiation Center at the Advanced Photon Source for their assistance in performing the experiments. The Argonne group is supported by the Chemical Sciences, Geosciences, and Biosciences Division and the Nuclear Physics Division of the Office of Basic Energy Sciences, Office of Science, U.S. Department of Energy, under Contract No. W-31-109-Eng-38. L.A.L. and R.H.P. are supported by National Science Foundation Grant No. 0201595. Use of the Advanced Photon Source is supported by the U. S. Department of Energy, Basic Energy Sciences, Office of Science, under Contract No. W-31-109-Eng-38.

---

[1] A. F. Starace, in *Handbuch der Physik, Vol. 31*, edited by W. Mehlhorn (Springer-Verlag, Berlin, 1982), pp. 1–121.

[2] V. Schmidt, Rep. Prog. Phys. **55**, 1483 (1992).

[3] J. G. Jenkin, J. Electron Spectrosc. Relat. Phenom. **23**, 187 (1981).

[4] J. Fischer, Ann. Phys. (Leipzig) **8**, 821 (1931).

[5] H. K. Tseng, R. H. Pratt, S. Yu, and A. Ron, Phys. Rev. A **17**, 1061 (1978).

[6] A. Bechler and R. H. Pratt, Phys. Rev. A **39**, 1774 (1989).

[7] A. Bechler and R. H. Pratt, Phys. Rev. A **42**, 6400 (1990).

[8] J. H. Scofield, Phys. Scripta **41**, 59 (1990).

[9] J. W. Cooper, Phys. Rev. A **47**, 1841 (1993).

[10] A. Derevianko, W. R. Johnson, and K. T. Cheng, At. Data Nucl. Data Tables **73**, 153 (1999).

[11] M. Y. Amusia, A. S. Baltenkov, L. V. Chernysheva, Z. Felfli, and A. Z. Msezane, Phys. Rev.

A **63**, 052506 (2001).

[12] M. Peshkin, Adv. Chem. Phys. **18**, 1 (1970).

[13] A. Derevianko, O. Hemmers, S. Oblad, P. Glans, H. Wang, S. B. Whitfield, R. Wehlitz, I. A. Sellin, W. R. Johnson, and D. W. Lindle, Phys. Rev. Lett. **84**, 2116 (2000).

[14] B. Krässig, M. Jung, D. S. Gemmell, E. P. Kanter, T. LeBrun, S. H. Southworth, and L. Young, Phys. Rev. Lett. **75**, 4736 (1995).

[15] M. Jung, B. Krässig, D. S. Gemmell, E. P. Kanter, T. LeBrun, S. H. Southworth, and L. Young, Phys. Rev. A **54**, 2127 (1996).

[16] V. Schmidt, *Electron Spectrometry of Atoms using Synchrotron Radiation* (Cambridge University, Cambridge, 1997).

[17] M. Peshkin, in *Atomic Physics with Hard X-Rays from High Brilliance Synchrotron Light Sources* (Argonne National Laboratory, ANL/APS/TM-16, 1996), pp. 207–217.

[18] M. A. Beno, G. Jennings, M. Engbretson, G. S. Knapp, C. Kurtz, B. Zabransky, J. Linton, S. Seifer, C. Wiley, and P. A. Montano, Nucl. Instrum. Methods A **467-468**, 690 (2001).

[19] P. S. Shaw, U. Arp, and S. H. Southworth, Phys. Rev. A **54**, 1463 (1996).

[20] M. Breinig, M. H. Chen, G. E. Ice, F. Parente, B. Crasemann, and G. S. Brown, Phys. Rev. A **22**, 520 (1980).

[21] N. M. Kabachnik and I. P. Sazhina, J. Phys. B **29**, L515 (1996).

[22] This expression is misprinted in Ref. [6].

[23] V. K. Dolmatov, A. S. Baltenkov, and S. T. Manson, Phys. Rev. A **64**, 042718 (2001).